Primary and secondary motoneurons use different calcium channel types to control escape and swimming behaviors in zebrafish

Hua Wen[a], Kazumi Eckenstein[a,1], Vivien Weihrauch[b], Christian Stigloher[b], and Paul Brehm[a,2]

[a]Vollum Institute, Oregon Health and Science University, Portland, OR 97239; and [b]Imaging Core Facility, Biocenter, University of Würzburg, 97074 Würzburg, Germany

Edited by Richard W. Aldrich, The University of Texas at Austin, Austin, TX, and approved September 4, 2020 (received for review July 27, 2020)

The escape response and rhythmic swimming in zebrafish are distinct behaviors mediated by two functionally distinct motoneuron (Mn) types. The primary (1°Mn) type depresses and has a large quantal content (Qc) and a high release probability (Pr). Conversely, the secondary (2°Mn) type facilitates and has low and variable Qc and Pr. This functional duality matches well the distinct associated behaviors, with the 1°Mn providing the strong, singular C bend initiating escape and the 2°Mn conferring weaker, rhythmic contractions. Contributing to these functional distinctions is our identification of P/Q-type calcium channels mediating transmitter release in 1°Mns and N-type channels in 2°Mns. Remarkably, despite these functional and behavioral distinctions, all ∼15 individual synapses on each muscle cell are shared by a 1°Mn bouton and at least one 2°Mn bouton. This blueprint of synaptic sharing provides an efficient way of controlling two different behaviors at the level of a single postsynaptic cell.

P/Q-type calcium channels | N-type calcium channels | synaptic | neuromuscular | conotoxins

The complex body plan associated with most classes of vertebrate animals provides for a wide repertoire of movements. This involves a large number of specialized muscle groups that serve different functions and are innervated by different spinal motoneurons (Mns). By contrast, fish largely conform to a simplified organization reflected in a segmentally repeating pattern of slow and fast axial muscle. Despite the simplicity of this organization, larval zebrafish are still capable of mounting distinct swimming behaviors that, through necessity, have evolved to use the same fast skeletal muscle cells. The principal behaviors correspond to a C bend, which mediates escape, and rhythmic swimming (1, 2). The C bend is likened to an all-or-none behavior, reflecting a single powerful stereotypic contraction. The ensuing rhythmic swimming covers a range of speeds that reflect differential power development using the same peripheral muscle cells as the C bend. The C bend is the most studied and best understood, due to both its simplicity and predictability (1, 3). The rhythmic swimming, however, involves control mechanisms that appear to govern contraction strength within and among muscle cells, a process that is considerably more complex.

It is generally agreed that the C bend is mediated by firing of the four large 1°Mns located in each spinal cord hemisegment (4, 5). By contrast, the rhythmic swimming reflects the distributed firing among the ∼40 2°Mn types within each hemisegment (6, 7). The principal control over rhythmic swimming falls to the 2°Mns with 1°Mns participating at only the fastest swim speed (4, 8). Unlike the stereotypic C bend, fine-tuning of swim speed involves a size-dependent recruitment among the 2°Mns (8, 9). Firing among the smallest, most ventral 2°Mns is causal to slow swimming whereas recruitment of more dorsal, larger size 2°Mns results in faster swimming (8). For the most part, studies on the mechanisms underlying Mn size dependence of swim speed have focused on distinctions in premotor spinal circuitry and intrinsic firing properties among the Mns (8–10). However, there is growing appreciation of peripheral mechanisms that also contribute to the regulation of power development. The first mechanism relates soma size to overall peripheral branching. A more extensive branching on the part of larger 2°Mns likely reflects a greater number of muscle cells receiving innervation (11), a proposition further supported by the present study. Accordingly, recruitment of larger Mns would result in increased power by activating a greater number of muscle cells. A second, and novel, peripheral determinant of swim speed was revealed through paired patch-clamp recordings of 2°Mns and target muscle (12). The recordings revealed a direct relationship between quantal content (Qc) and 2°Mn size at the level of individual muscle cells. Consequently, a larger Qc would aid in contraction strength by producing a greater depolarization in the muscle cells targeted by the larger 2°Mns (12). The bases for these peripheral distinctions are explored in greater detail in the present study.

To address more directly the links between peripheral circuitry, Qc, and behavior, we have used direct imaging and in vivo paired recordings. This has led to identification of distinct calcium channel types mediating synaptic transmission in the two Mn types as well as an organization involving sharing of synapses by both 1° and 2°Mn boutons. Moreover, the functional distinctions between 1° and 2°Mn boutons control two behaviors through shared synapses on the same muscle cell. Our identification of the sharing of synapses by functionally dichotomous

Significance

Genetic manipulations, functional imaging, and patch-clamp electrophysiology provide new insights into the roles played by the P/Q and N calcium channel types in zebrafish neuromuscular transmission. These two channel types are the mainstay of synaptic transmission among vertebrates and their functional distinctions likely form the basis of their synapse-specific expression. We show that the primary and secondary motoneurons differ in these two calcium channel types, providing independent control over escape and rhythmic swimming behaviors. The control over separate behaviors occurs despite their sharing of the same synapses and postsynaptic receptors. This synapse sharing by presynaptic terminals with functionally distinct calcium channel types calls for investigations into similar processes at other synapses.

Author contributions: H.W., C.S., and P.B. designed research; H.W., K.E., and V.W. performed research; H.W., K.E., V.W., C.S., and P.B. analyzed data; and H.W. and P.B. wrote the paper.

The authors declare no competing interest.

This article is a PNAS Direct Submission.

[1]Present address: Department of Developmental and Cell Biology, University of California, Irvine, CA 92697.

[2]To whom correspondence may be addressed. Email: brehmp@ohsu.edu.

First published October 5, 2020.

boutons calls for investigation into the existence of a similar plan among the neurons of the vertebrate CNS.

Results

Innervation Pattern and Distribution of 1° and 2°Mn Synapses. Early electrophysiological recordings indicated that single fast muscle fibers receive innervation from a single 1°Mn and up to three additional 2°Mns (7). The distribution of synapses among fast muscle fibers is well-documented for the 1°Mn types. The fast muscle is segregated into four quadrants within each segment, each bearing nonoverlapping innervation by one of four different 1°Mns (6, 7, 11). Our studies have focused on the caudal primary (CaP) 1°Mn, which branches extensively to innervate all of the muscle cells in the ventral most quadrant (Fig. 1*A*). Labeling with either fluorescently conjugated alpha bungarotoxin (α-Btx) or postsynaptic rapsyn, tagged with either the calcium indicator GCaMP6f or green fluorescent protein (GFP), reveals an en passant distribution of postsynaptic acetylcholine receptor (AChR) clusters that number ∼15 per muscle cell (Fig. 1 *A* and *B*) (13, 14). Much evidence points to each cluster as representing an individual synapse formed with the 1°Mn. Morphologically, each of the ∼15 receptor clusters colocalizes with a fluorescence-labeled 1°Mn terminal (Fig. 1*B*). Paired recordings and variance analysis of endplate currents (EPCs) also provided support for a one-to-one correspondence between 1°Mn terminals and receptor clusters (14). A direct test of the proposition that the 1°Mn innervates each individual receptor cluster formed on target muscle is now provided using an optical strategy (Fig. 1 *C* and *D*). Transmitter release at individual synapses was monitored during CaP 1°Mn stimulation by GCaMP6f, targeted to postsynaptic sites via fusion to rapsyn (Fig. 1*B*). To ensure that changes in fluorescence signal reflect calcium influx through the AChR during synaptic activity and not depolarization-mediated release from intracellular stores, the measurements were made using the muscle dihydropyridine receptor mutant *relaxed* (15, 16). Owing to the high fractional calcium permeability of the AChR, our resolution was sufficient to detect single fusion events (Fig. 1*C*). Stimulation of the CaP 1°Mn at 0.2 Hz led to detectable GCaMP6f signals at every synapse on individual muscle cells (Fig. 1 *C* and *D*). Through monitoring of the failures, this assay also allowed direct measurements of the release probability (Pr) at individual synapses (Fig. 1 *D* and *E*). Consistent with the findings from paired recordings, Pr was near unity for each synapse (14). Collectively, these findings point to occupancy of nearly all synapses by the 1°Mn, raising the intriguing question as to the location of those synapses corresponding to the 2°Mns.

We sparsely labeled 2°Mns with transient expression of fluorescent proteins to facilitate reconstruction of branching patterns for individual 2°Mns. Consistent with a recent publication, we identified a broad range of branching patterns, from simple to highly complex, among the over 40 2°Mns (11) (Fig. 2*A*). Both the extent of branching and synapse numbers was directly related to soma size (Fig. 2*A*). These findings indicate that larger 2°Mns innervate a larger number of muscle cells, accounting in part for the size dependence of power production.

To examine the location of 2°Mn synapses relative to those of the 1°Mn, sparse labeling of 2°Mns was performed in a transgenic line expressing enhanced GFP (EGFP) specifically in the CaP 1°Mn. Single 2°Mns that branch into ventral target territory of the CaP 1°Mn were imaged along with the CaP arbor and α-Btx–labeled AChR clusters (Fig. 2 *B* and *C*). Coincidence labeling of AChR clusters with the terminals of both the CaP 1°Mn and 2°Mn pointed to frequent sharing of synapses between the two Mn types (Fig. 2*B*). To quantitate the extent of sharing, three-dimensional reconstruction was performed for the synapses in the CaP target territory for both Mn types (Fig. 2*C*). As expected, over 99% of all synapses in this region were associated with the CaP (Fig. 2 *C, 1*; 99.4 ± 0.5%, $n = 13$). In addition, ∼98% of the receptor clusters associated with the labeled 2°Mn (Fig. 2 *C, 2*) colocalized with those of the CaP (Fig. 2 *C, 3* and *4*; 97.9 ± 1.6%, $n = 13$). Because this experiment labeled only one of the 2°Mns that extended branches into the CaP territory, those CaP synapses that were scored as not shared (green in Fig. 2 *C, 3*) are shared with a different unlabeled 2°Mn and/or occupied solely by the CaP.

This method did not provide information as to how many 2°Mns share individual synapses with a 1°Mn. For this purpose, we turned to conventional electron microscopy to count the bouton number at individual synapses. To satisfy the criteria for a synapse, we required that there be evidence of electron-dense material between muscle and nerve as well as accumulation of synaptic vesicles (Fig. 2*D*). The overall distribution determined for six fish ranged from one to three boutons ($n = 52$ synapses) (Fig. 2*D*). Assuming that in all cases one of the boutons corresponds to the 1°Mn, we interpret these data as representing between zero and two boutons of 2°Mns at each synapse, with a major mode of one. It is likely that these counts represent an underestimate due to missed Mn boutons out of registry during sectioning.

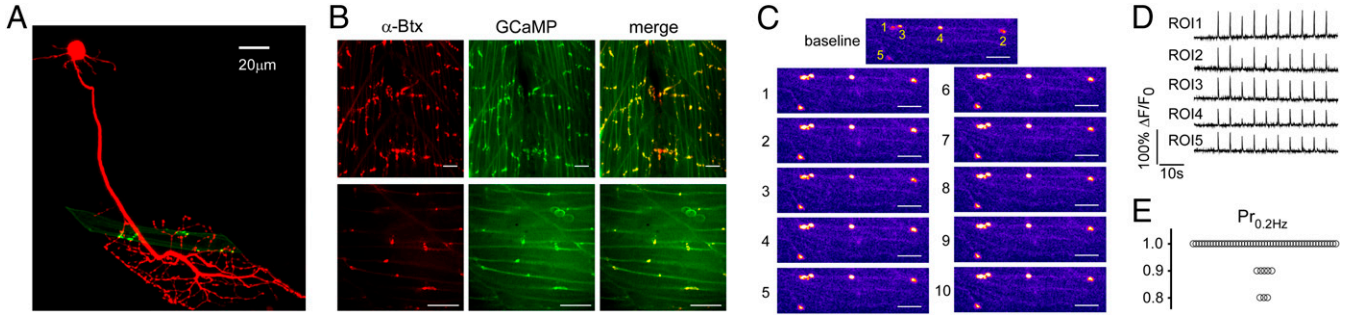

Fig. 1. CaP 1°Mn occupies nearly all of the synapses formed on individual muscle cells. (*A*) Maximal projection of confocal images of a CaP (red) and an example target muscle with its associated receptor clusters (green). The CaP was labeled with tdTomato expression driven by the mnx1 promoter. Postsynaptic receptors were labeled with rapsyn-GFP driven by the α-actin promoter that sparsely labeled muscle cells. (*B*) Confocal *Z*-stack maximal projection (*Top*) and single focal plane (*Bottom*) images of approximately two segments showing colocalization of AChR labeling with α-Btx (red) and rapsyn-GCaMP6f basal fluorescence (green). (Scale bars, 20 μm.) (*C*) Example GCaMP6f fluorescence responses for five synapses in response to 0.2-Hz stimulation of the CaP (10 consecutive responses are shown). In this focal plane, ROIs 1 to 4 are located in the same muscle cell, while ROI 5 is on a different muscle. Scale bars, 15 μm. (*D*) Individual GCaMP6f responses for the five ROIs in response to 0.2-Hz stimulation of the CaP. (*E*) Overall distribution of Pr at 0.2 Hz measured for 59 ROIs from 16 fish.

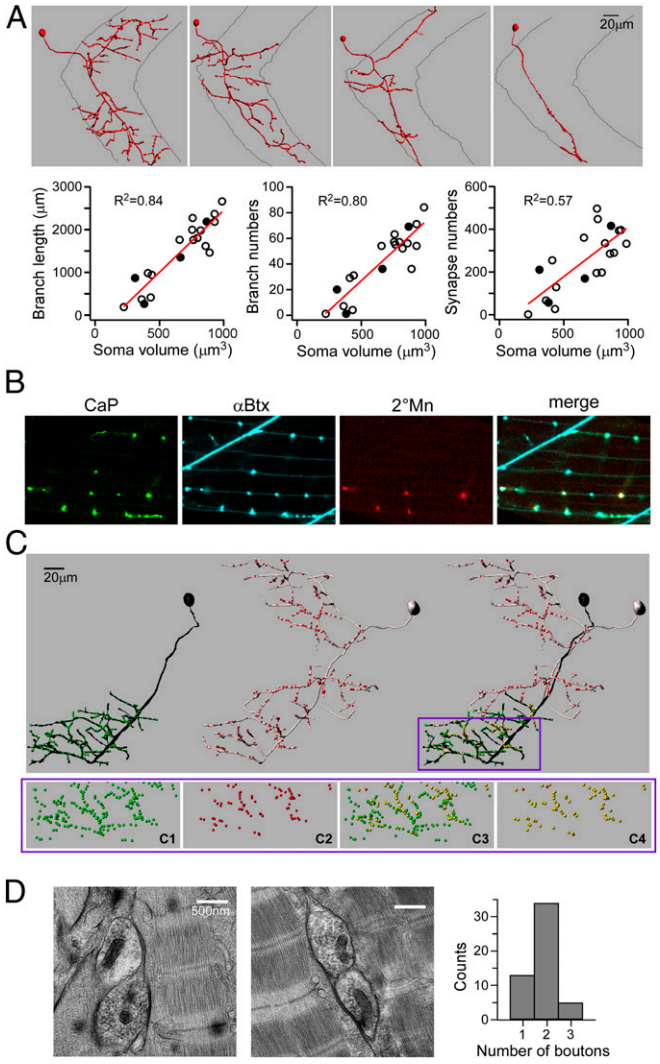

Fig. 2. Sharing of synapses by 1° and 2°Mns. (*A*) Imaris reconstructions of four different 2°Mns exemplifying the range of axonal branching patterns (*Top*). Relationships between soma volume versus axonal branch length, branch number, and α-Btx punctum number are shown (*Bottom*). Each symbol represents a reconstruction of an individual 2°Mn, with filled symbols corresponding to the four examples shown. The relationship shows a linear fit with R^2 values indicated. (*B*) Confocal images showing colocalization of fluorescently labeled CaP terminals (green), postsynaptic AChR (cyan), 2°Mn terminals (red), and merge. CaP is labeled with EGFP expression driven by the SAIG213A Gal4 promoter. A single 2°Mn is labeled with tdTomato expression driven by the mnx1 promoter. (*C*) Imaris reconstruction of a 1°Mn (black) and a 2°Mn (gray). Individual synapses, based on the α-Btx label, are color-coded in green (for 1°Mn), red (for 2°Mn), and yellow (scored as shared). Only the bottom half of the ventral muscle field is considered for quantitation as CaP is the sole 1°Mn innervating that area. (*C*, *Bottom*) An expanded view of the boxed region shows the distribution of synapses that are associated with CaP (*C1*) or 2°Mn (*C2*) or scored as shared among all synapses (*C3*) or in relation to the 2°Mn synapses (*C4*). In this example, 98% of the labeled 2°Mn synapses in the overlapping region were shared with the CaP. (*D*) Example electron micrographs showing two boutons sharing a synapse. (*D*, *Right*) Histogram of 52 images from six fish is shown.

Functional Distinctions between 1°Mn- and 2°Mn-Mediated Neuromuscular Transmission. Paired recordings between target muscle and either the CaP 1°Mn or a 2°Mn revealed Mn-specific differences in neuromuscular transmission (Fig. 3). As shown by use of optical recordings (Fig. 1) and published recordings, the CaP 1°Mn has near-unity Pr at low stimulus frequency. As such, it represents a fast depressing synapse when the stimulus frequency is increased (14). It also has a Qc of ∼15 that matches the estimated number of functional release sites and the number of postsynaptic receptor clusters (Fig. 3*A*) (14). By contrast, the 2°Mn has smaller and highly variable Qc (Fig. 3 *A* and *C*) (12). For quantitative comparison of synaptic strength with the CaP 1°Mn, we chose a specific subgroup of 2°Mns that extends branches into both dorsal and ventral muscle segments with an input resistance in the range of 250 to 500 MΩ (one example shown in the first panel of Fig. 2*A*) (11). EPC amplitudes for the 2°Mn showed large fluctuations along with frequent failures (34 ± 27% failure rate, $n = 21$; Fig. 3*B*). These fluctuations in amplitude translate directly to differences in Qc based on similar mean miniature EPC (mEPC) amplitudes for both Mn types (Fig. 3*C*). The mEPC amplitude was determined for each Mn using isolated unitary events that are not synchronous with action potential firing, taking advantage of the fact that high-frequency stimulation led to an elevated occurrence of asynchronous mEPCs (14, 17). The mean amplitudes corresponded to 945 ± 216 pA ($n = 20$) for the 1°Mn and 926 ± 155 pA ($n = 14$) for the 2°Mn. Based on the direct method (mean EPC amplitude/mean mEPC amplitude), the Qc averaged 1.2 ± 1.0 ($n = 21$) for the 2°Mn and 12 ± 3.2 ($n = 26$) for the CaP 1°Mn. The difference in synaptic strength between Mn types reflects the much lower Pr in 2°Mns compared with 1°Mn synapses. The Pr in the 2°Mn can be further facilitated during repetitive stimulation, resulting in reduced occurrence of failure and increased EPC amplitudes (average fold of increase 2.1 ± 0.6, $n = 12$; Fig. 3*D*).

The EPCs for the two Mn types have similar rise and decay times but the onset of the EPC is delayed in the 2°Mn when compared with the 1°Mn. Measured as the interval between the peak of the Mn action potential and 10% rise of the EPC, the synaptic delay averages 1.43 ± 0.11 ($n = 21$) for the 2°Mn compared with 0.69 ± 0.06 ($n = 26$) for the 1°Mn, corresponding to a 2.1-fold difference (Fig. 3*E*). Additionally, there are greater variations in the synaptic delay for the 2°Mn EPCs (Fig. 3*F*). Overall, 2°Mn synapses are weaker in strength and less reliable and lack the temporal precision of 1°Mn synapses.

Synaptic Transmission and Behavior in a P/Q Calcium Channel-Null Mutant. Assignment of P/Q calcium channels as mediators of 1°Mn neuromuscular transmission was based on a mutant line harboring a missense mutation in the P/Q channel (18). This mutant showed greatly reduced levels of neuromuscular transmission in vivo and compromised swimming, both of which we attributed to the residual levels of P/Q expression (18). We have subsequently obtained a second P/Q mutant line that represents a complete null due to premature truncation of the channel and this has provided insights into functional distinctions among Mn types. The first hints came from monitoring of electrical stimulation-induced escape and swimming using high-speed imaging (Fig. 4). Wild-type fish responded to a brief shock with an initial powerful C bend characterized by a high degree of curvature corresponding to 131 ± 22° (Fig. 4 *A* and *B*; $n = 12$ fish). This bend was followed by a bout of rhythmic swimming with alternating tail beats that decreased in strength and duration. In the P/Q-null fish the initial bend reached only ∼1/3 of the curvature measured for the C bend in wild-type fish (49 ± 15°, $n = 14$; Fig. 4 *A* and *B*). Additionally, the onset of the first body bend was delayed compared with wild-type fish (Fig. 4 *A* and *C*; 21.0 ± 4.5 ms, $n = 12$ for wild type; 39.4 ± 5.4 ms, $n = 14$ for P/Q-null). This delay of 18.4 ms compared favorably with the average duration of the C bend for wild-type fish (19.1 ± 6.4 ms, $n = 12$). These measurements demonstrated that P/Q-null mutants lack the C bend while maintaining the ability to mount rhythmic swimming.

Using paired recordings, we revisited previously published evidence pointing to reliance on P/Q-type calcium channels in neuromuscular transmission between the 1°Mn and target

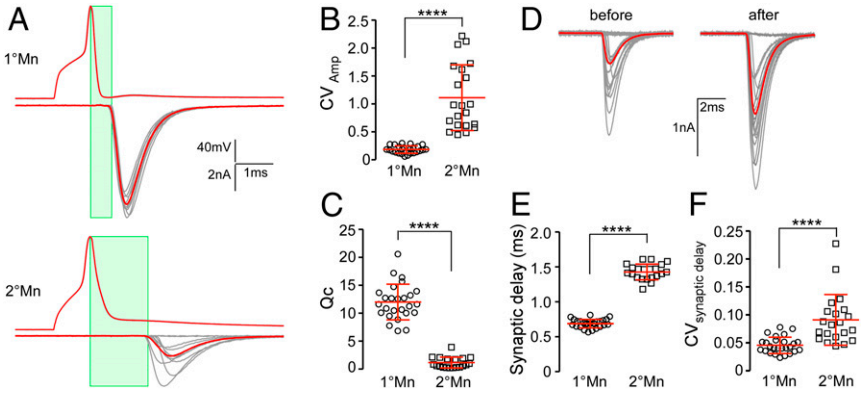

Fig. 3. Functional distinctions between 1° and 2°Mn synapses. (*A*) Example traces of action potentials and EPCs (average in red) for CaP 1°Mn and 2°Mns in response to 10 stimuli at 1 Hz. The time window for synaptic delay measurement is shown (in green). (*B*) Scatterplot comparing the coefficient of variation (CV; mean ± SD in red) for EPC amplitudes between the 1° and 2°Mns. CV is calculated for 20 responses acquired at 1 Hz for each cell. (*C*) Scatterplot comparing quantal content (mean ± SD in red) between 1° and 2°Mns. (*D*) A sample 2°Mn paired recording showing 20 EPCs at 1-Hz stimulation before and after facilitation (average in red). The facilitation was induced with a 100-Hz, 2-s stimulus train in the 2°Mn. (*E*) Scatterplot comparing the synaptic delay (mean ± SD in red) between 1° and 2°Mns. (*F*) Scatterplot comparing CV (mean ± SD in red) for the synaptic delay between 1° and 2°Mns. ****$P < 0.0001$.

muscle. The total charge transfer for 20 responses at 1 Hz corresponded to 0.55 ± 0.59 pC ($n = 17$) in the P/Q-null mutants, compared with 204 ± 71 pC ($n = 29$) for wild-type fish, reflecting a >99% reduction of synchronous release in the CaP 1°Mn in the absence of functional P/Q channels (Fig. 5 *A* and *B*).

As 2°Mns have been shown to be central to rhythmic swimming, we performed paired recordings between 2°Mns and target muscle in the P/Q-null mutants. In contrast to the absence of release in the 1°Mns, evoked synaptic transmission was intact between 2°Mn and target muscle (Fig. 5 *C* and *D*). Comparison of total release showed no statistically significant difference between wild-type and P/Q-null fish (Fig. 5*D*; 17.7 ± 15 pC, $n = 20$ for wild type and sibling; 11.0 ± 7.8, $n = 22$ for mutants; $P = 0.07$). Overall, our electrophysiology and behavior measurements indicate that a calcium channel other than the P/Q type mediates neuromuscular transmission in the 2°Mns.

Identifying the Calcium Channel Type Used for Synaptic Transmission in 2°Mns. The zebrafish P/Q channel type has a pharmacological profile that sets it apart from its mammalian counterpart (18). Specifically, zebrafish P/Q channels are sensitive to ω-conotoxin GVIA, a toxin widely considered to be N type-specific. ω-Conotoxin GVIA blocked both zebrafish P/Q-type and N-type currents in a heterologous expression system as well as abolishing CaP 1°Mn synaptic transmission in vivo (18). To test the effect of the toxin on 2°Mn-mediated synaptic transmission, we used a line of fish expressing channelrhodopsin (ChR) principally in the 2°Mns (19). Recordings revealed that application of 1 μM ω-conotoxin GVIA blocked all of the light-evoked responses ($n = 4$). Additionally, injection of ω-conotoxin GVIA into fish leads to total paralysis of the animal ($n = 15$). On the basis of sensitivity to ω-conotoxin GVIA and having ruled out the P/Q type, we tested for N-type calcium channel involvement in 2°Mn-mediated neuromuscular transmission.

To date, efforts to identify or generate zebrafish N and P/Q subtype-specific antibodies have failed, due largely to the high sequence similarity between the channel types. As an alternative means, we turned to a panel of nine ω-conotoxins that have been tested on mammals to be N type-specific (Alomone Labs) in search for a toxin with differential blocking effect on zebrafish N and P/Q channels. The toxins were first tested for their effectiveness on blocking 2°Mn-mediated synaptic transmission. For this purpose, high concentrations (1 to 5 μM) of each toxin were applied to fish expressing ChR in 2°Mns, and light-evoked responses were recorded in the muscle. Four toxins showed no evidence of block and were not subjected to further testing (ω-conotoxins CVIA, SVIB, SO3, and FVIA; Table 1). The remaining five toxins strongly blocked 2°Mn transmission and were then tested for specificity in paired recordings between the CaP 1°Mn and target muscle. Application of ω-conotoxins RVIA and MVIIA also blocked CaP-mediated transmission, indicating that they act on both the zebrafish P/Q- and N-type channels, and were not further tested. By contrast, ω-conotoxins CVIE, CVIF, and CnVIIA showed greatly reduced sensitivity on the CaP 1°Mn release compared with their effects on 2°Mn-mediated transmission. Consequently, they served as candidates for specific block of the putative N-type channel responsible for 2°Mn transmission (Table 1). Two of these were used for further studies.

To confirm a preferential block of the N type, we quantitated the potency of the toxins on zebrafish N- and P/Q-type channels

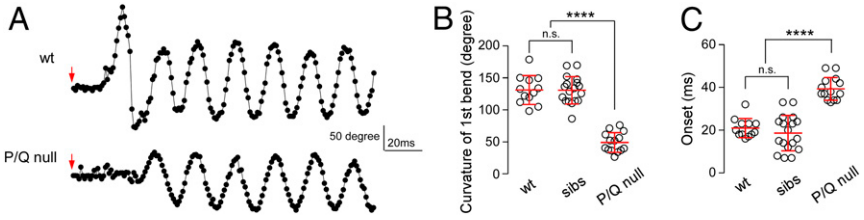

Fig. 4. P/Q-type channel-mediated transmission specifically supports the escape response. (*A*) Example time series showing changes in body curvature during responses triggered by a 20-ms electrical field stimulation (arrows are the start marks) of a wild-type (wt) and P/Q-null fish. Movies were acquired at 1,000 frames per second and analyzed using Flote motion analysis software. (*B*) Scatterplot comparing curvature of the first bend for wild type, siblings, and P/Q-null mutants. (*C*) Scatterplot comparing the onset of movement for wild type, siblings, and P/Q-null mutants. Heterozygous siblings were indistinguishable from wild type. n.s., not significant, with *P* values greater than 0.05. Mean ± SD is indicated in red. ****$P < 0.0001$.

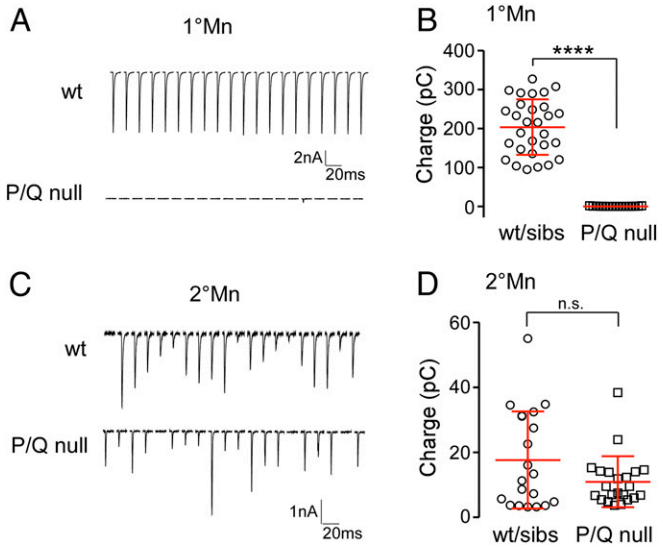

Fig. 5. P/Q-null mutant specifically abolished synaptic transmission in 1°Mns. (*A*) Example traces of 20 consecutive EPC responses at 1 Hz in the CaP 1°Mn from a wild type (*Top*) and a P/Q-null mutant (*Bottom*). (*B*) Scatterplot comparing the total charge transfer for 20 responses at 1 Hz in the CaP 1°Mn between wild type and P/Q-null mutants. Mean ± SD is indicated in red. ****$P < 0.0001$. (*C*) Example traces of 20 consecutive EPC responses at 1 Hz in a 2°Mn from a wild type (*Top*) and a P/Q-null mutant (*Bottom*). (*D*) Scatterplot comparing the total charge transfer for 20 responses at 1 Hz in wild type and P/Q-null mutants. Mean ± SD is indicated in red. n.s. corresponds to $P = 0.07$. Heterozygous siblings were indistinguishable from wild-type fish, and data were pooled in the summary plots.

expressed in human embryonic kidney 293T (HEK293T) cells (Fig. 6) (18). For each toxin at least four concentrations were tested for block of calcium current. The half-maximal inhibitory concentrations (IC_{50}s) were compared between the two channel types (Fig. 6*A*). The higher-affinity CVIF showed a 6.8-fold preference for block of the N type with an IC_{50} corresponding to 44 nM for the N type and 301 nM for the P/Q type (Fig. 6*B*). The lower-affinity blocker CnVIIA showed a 2.7-fold difference, with the IC_{50} corresponding to 904 nM for the N type and 2.4 μM for the P/Q type (Fig. 6*C*).

With the concentration dependencies for N versus P/Q channel block in hand, we turned to in vivo paired recordings to test for selective actions on 2°Mn- and 1°Mn-mediated synaptic transmission (Fig. 7). For this purpose, ω-conotoxin CVIF was selected because it provided the greatest distinction between the channel types expressed in HEK293T cells. At 200 nM, CVIF blocked ~90% of N-type and less than 20% of P/Q-type calcium current (Fig. 6 *A* and *B*). EPCs were recorded for each Mn type before and after a solution change to 200 nM CVIF. The blocking actions at this concentration approximated the results obtained from expressed channels with an average block of 21.7 ± 7.6% ($n = 5$) for the CaP 1°Mn and 73.5 ± 8.5% ($n = 5$) for the 2°Mn (Fig. 7). Quantitative comparison between block of the calcium current in HEK293T cells and reduction of transmitter release in vivo cannot be made without knowledge of calcium dependence of exocytosis at the zebrafish neuromuscular junction (NMJ). Overall release of the transmitter generally has a steep nonlinear dependence on calcium influx (20). However, at some synapses, openings by single calcium channels are able to promote fusion of individual vesicles in an all-or-none fashion, predicting a linear dependence on calcium entry (21–24). Regardless of this uncertainty, the differential action of ω-conotoxin CVIF in vivo supports reliance of 2°Mn-mediated neuromuscular transmission on N-type calcium channels.

Discussion

When first published, our identification of a zebrafish P/Q calcium channel as the mediator of neuromuscular transmission came as a surprise (18). Frog NMJs had long been associated with reliance on an N-type calcium channel based on sensitivity to ω-conotoxin GVIA and MVIIC, setting it apart from mammalian NMJs that used a P/Q type (25–28). However, such a distinction has always been difficult to reconcile in light of such an otherwise highly conserved synapse among vertebrates. Pharmacological testing of ω-conotoxin GVIA, presumed to be N type-specific, on heterologously expressed zebrafish P/Q- and N-type calcium channels provided a potential resolution (18). Both channel types showed similar blocking profiles, pointing to a potential misidentification in frog and to common usage of a P/Q type among all vertebrates.

Subsequent paired recordings from CaP 1°Mn and target muscle from a P/Q channel mutant lent strong support for the reliance of zebrafish neuromuscular transmission on this channel type (18). One caveat, however, was reflected in the ability of the P/Q mutant line to retain limited motility. At the time it was reasoned that the mutant line was not a complete null. The recently obtained P/Q mutant line used in the present study was able to mount rhythmic swimming, despite the prediction that it represents a functional null. This finding, together with the observation that all swimming movement was completely blocked by ω-conotoxin GVIA, raised the likelihood of an N-type calcium channel as mediator of release in the 2°Mn, the Mn type that controls rhythmic swimming. This proposition was confirmed by paired recordings at 2°Mn synapses in the P/Q-null mutants, and further supported by our identification of a conotoxin that preferentially inhibited N-type calcium channels and synaptic transmission by 2°Mns.

Table 1. Exploratory screen for toxins that distinguish between zebrafish N-type and P/Q-type calcium channels

Toxin	ChR-YFP response	CaP release	Likely outcome
ω-Conotoxin CVIA	Not blocking at 1 μM	N.D.	Neither N- nor P/Q-blocking
ω-Conotoxin SVIB*	Not blocking at 1 μM	Not blocking at 1 μM	Neither N- nor P/Q-blocking
ω-Conotoxin SO3	Not blocking at 1 μM	N.D.	Neither N- nor P/Q-blocking
ω-Conotoxin FVIA	Not blocking at 1 μM	N.D.	Neither N- nor P/Q-blocking
ω-Conotoxin RVIA	Strong block at 2 μM	Strong block at 2.6 μM	Both N- and P/Q-blocking
ω-Conotoxin MVIIA	Strong block at 1 μM	Nearly complete block at 1 μM	Both N- and P/Q-blocking
ω-Conotoxin CVIE	Strong block at 1μM	Slight block at 330 nM	N-specific
ω-Conotoxin CVIF	Strong block at 1 μM	Residual response at 1 μM, 500 nM, 330 nM	N-specific
ω-Conotoxin CnVIIA	Strong block at 5 μM	Slight block at 2.5 μM	N-specific

N.D., not determined.
*When tested subsequently on the basis of behavior, ω-conotoxin SVIB caused paralysis, indicating it has actions beyond calcium channels, likely directly on muscle.

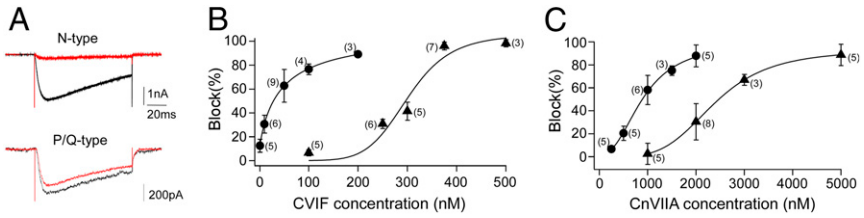

Fig. 6. Two ω-conotoxins that distinguish zebrafish N- and P/Q-type calcium channels. (*A*) Sample recordings of calcium currents from HEK293T cells expressing zebrafish P/Q- or N-type channels, before (black) and after (red) application of ω-conotoxin CVIF; 200 and 250 nM of toxin were applied for N and P/Q, respectively. (*B*) Dose–response curve of ω-conotoxin CVIF block on N (circles) and P/Q (triangles) currents. (*C*) Dose–response curve of ω-conotoxin CnVIIA block on N (circles) and P/Q (triangles) currents. For the dose–response curve, each symbol represents the average of multiple applications for the indicated number of different cells tested. The average values for all cells tested at each concentration are shown along with SD. Each relationship was fit by a Hill equation.

Our finding that the P/Q-null mutants specifically lacked a C bend is consistent with published studies pointing to principal control by the 1°Mns (4, 5). However, the complete absence of the C bend represents clear evidence that the 2°Mns do not participate significantly in that behavioral response and are relegated to rhythmic swimming. The behavioral responses controlled by the 1° and 2°Mn types are well-accounted for by the differences in Qc between Mn types and consequential differences in contraction strength. This is due in part to the peripheral circuitry where small-sized 2°Mns contact fewer muscle cells, thereby generating less power and slower swimming (Fig. 2*A*) (11). In addition, the smaller Mns also have smaller Qc, leading to the generation of weaker contractions at the level of individual muscle cells (12). The small zebrafish muscle cells are nearly isopotential due to a high input resistance, thereby distributing the synaptic depolarization throughout the cell. The 1°Mn produces the largest depolarization due to the large Qc which helps insure that the C bend generates the most power and the fast depression insures that only a single such response is generated. By contrast, the 2°Mns vary greatly in their Qc, accounting for a graded depolarization and release of intracellular calcium in muscle (12). This enables graded power development for rhythmic swimming that spans a range of speeds.

What features of the N versus P/Q calcium channel types might account for the Mn-specific differences in Pr? First, the distinction could reflect the intrinsic biophysical properties of the channels. At zebrafish NMJs and mouse mossy fiber synapses, the P/Q type has a higher open probability than the N type, which would be expected to result in greater action potential-associated calcium influx (29, 30). Second, the distinctions in Pr could result from differences in the density of calcium channels (31–34). For example, should P/Q channels occur at higher density, the local calcium domains may show greater overlap, thus increasing the calcium available for release (35). Third, the location of the P/Q- versus N-type calcium channels may differ in relation to the release machinery. Spatial arrangements play critical roles in setting the coupling between calcium influx through the channel and vesicle release (21, 24, 36, 37). Tighter coupling has been shown for several central synapses that rely on the P/Q type, while looser coupling is often associated with weaker synapses that use the N type for release (23, 38–42). The P/Q- and N-type channels differentially interact with multiple proteins in the exocytotic machinery and other active zone components (43–45), providing a potential molecular mechanism contributing to differences in localization and coupling.

Innervation of individual muscle cells by functionally dichotomous Mns, as reported here, has also been identified at the larval wall muscles in *Drosophila* (46). There, the 1s and 1b Mns innervate the same muscle cells but differ in terms of reliability and fatigue. The 1s synapses are reliable and depress compared with 1b synapses that are often largely silent and "wake up" in response to high-frequency stimulation (46). Thus, the 1s is similar to the 1°Mn type and the 1b to 2°Mns that show frequent failure. The functional distinctions at the fly NMJ have been shown to involve postsynaptic glutamate receptor composition and presynaptic differences in calcium channel density as well as the levels of the active zone organizer *bruchpilot* (47). At zebrafish NMJs, we can rule out involvement of postsynaptic receptors in the distinction because of synapse sharing. The zebrafish NMJ offers some significant advantages over flies in the hunt for mechanisms regulating Pr. Simplicity is provided by the low number of synapses per muscle cell (~15 vs. hundreds in the fly), the large size of individual synapses which precludes the need for superresolution methodology, and the amenability to paired patch-clamp Mn–muscle recording (13). Additionally, sharing of 1° and 2°Mn boutons at the same synapse offers the opportunity for side-by-side interrogation of high- and low-Pr synapses for differences at the molecular and ultrastructural levels. High-pressure freezing electron microscopic tomography of zebrafish NMJs, for example, will offer the opportunity to test for differences in presynaptic organization between the two Mn types (48).

The sharing of individual neuromuscular synapses by multiple Mns is not without precedent among vertebrates. During early development and reinnervation following injury, multiple different Mns share the same synaptic gutter and receptors (49). Through a process of competition, Mns sequentially withdraw over the course of development until only one Mn terminal remains at every synapse (50). The mechanisms causal to the

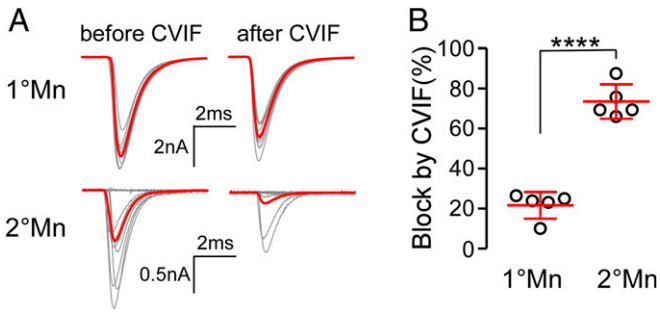

Fig. 7. N type-specific ω-conotoxin CVIF preferentially blocks transmitter release in 2°Mn. (*A*) Example paired recordings showing block of EPCs by CVIF in 1° and 2°Mns. Ten EPCs along with the average (in red) at 1-Hz stimulation are shown before and after application of 200 nM toxin. Decreased responses in 2°Mns were accompanied by an increased failure rate, with the smallest responses representing miniature EPCs. (*B*) Scatterplot comparing CVIF block in 1° and 2°Mn EPC recordings. Synaptic responses were quantified as the summed charge transfer of 20 EPCs. Mean ± SD is indicated in red. ****$P < 0.0001$.

competition remain uncertain but evidence points to differences in synaptic strength (51–53). Our data from zebrafish NMJs showing a preponderance of a single 2°Mn co-occupying each synapse along with the 1°Mn support a competition among 2°Mns. This would indicate that whatever mechanisms are responsible for competition within a class of Mns do not apply to 1°Mns versus 2°Mns. This could potentially play a central role in establishment of stereotypic peripheral circuitry through timed outgrowth and competition. According to this model the axons of the 1°Mns, which are the first to emerge from the spinal cord, are followed by timed outgrowth of the numerous 2°Mns. We propose that the first 2°Mns to emerge would be the most branched and co-occupy the greatest number of synapses due to availability; 2°Mns emerging later would co-occupy fewer synapses due to prior occupancy by another 2°Mn. In this manner, a stereotypic innervation pattern could potentially be formed through precisely timed outgrowth of 2°Mns, with those bearing the fewest branches and synapses reflecting the last to emerge from the spinal cord.

This study links different behaviors to expression of N versus P/Q calcium channel types. These two channel types are the most common types used for synaptic transmission in the central nervous system (CNS) and confer functional distinctions in synaptic transmission (54). In the case of the zebrafish NMJ, the functional distinctions are reflected in a high-Pr bouton that mediates a powerful C bend via a P/Q calcium channel and graded swimming speed through a low-Pr–facilitating bouton that uses an N-type channel. The unexpected finding that functionally dichotomous boutons share the same synapse is without precedent in the CNS, but our findings now raise the possibility that synapse sharing at excitatory or inhibitory central synapses exists but has gone undetected.

Materials and Methods

Fish Lines. All zebrafish (*Danio rerio*) were maintained in the in-house facility. The P/Q-null mutant fish line (cacna1ab~sa35120) was obtained from the Sanger Institute's Zebrafish Mutation Project (55) (Zebrafish International Resource Center). It harbors a nonsense mutation that truncates the protein at amino acid 372 (out of a full length of 2,280). Zebrafish husbandry and procedures were carried out according to the standards approved by the Institutional Animal Care and Use Committee at Oregon Health and Science University. All experiments were performed using larvae at 72 to 120 h post fertilization (hpf). The sex of the larvae was unknown at this age.

Motoneuron Labeling and Reconstruction. A double-transgenic line, SAIGFF213A; UAS:EGFP, provided the labeling of the CaP 1°Mn. It expresses EGFP in a subset of spinal neurons, exclusively in CaP in some segments (56). For sparse labeling of the 2°Mn, we transiently expressed mCherry-tagged synaptotagmin 2 driven by the neuronal specific HuC promoter by injecting the plasmid into single-cell embryos. In some experiments, the Gal4-UAS system was used to achieve mosaic expression by coinjection of two DNA plasmids. In those cases, the mnx1 promoter drove the expression of Gal4 in motoneurons (mnx1:Gal4 plasmid, kindly provided by David McLean, Northwestern University, Evanston, IL) and a red fluorescent protein containing UAS construct served as the reporter (UAS:tdTomato or UAS:Cytobow plasmid, kindly provided by Tamily Weissman-Unni, Lewis & Clark College, Portland, OR). Injected wild-type fish were screened at 72 to 96 hpf for single fluorescent 2°Mns that could provide detailed morphology. For experiments investigating synapse sharing between Mn types, injected SAIGFF213A; UAS:EGFP larvae were screened for candidates containing segments where a single 2°Mn shared an overlapping target field with the CaP 1°Mn. Candidate fish were subsequently injected in the aorta with 0.5 nL of 1 mg/mL CF405s-conjugated α-Btx (Biotium) and allowed 15 to 30 min to label AChR clusters before mounting for imaging.

Z-stack images of labeled Mns and α-Btx–labeled AChR clusters were acquired using a laser-scanning confocal microscope (Zeiss LSM 710) with a C-Apochromat 40×/1.2-W objective. The *z*-stack images of somata and axon branches were reconstructed using Imaris 9.0 filament software (Bitplane). α-Btx punta were detected using the Spots function and annotated as spheres of 2-μm radius. To associate a postsynaptic receptor cluster with either Mn type, a maximum of 1-μm distance between a neuronal branch and individual α-Btx puncta was used as the criteria.

Optical Monitoring of Neuromuscular Transmission at Single Synapses with GCaMP6f. Our transgenic line targeting the genetically encoded calcium sensor GCaMP6f (57) to postsynaptic receptor clusters was used to monitor neurotransmitter release at individual single synapses. GCaMP6f was fused to the C terminus of the AChR-clustering protein rapsyn, and fusion protein expression was driven with the muscle-specific α-actin promoter. To ensure the fluorescence change is not complicated by calcium release from intracellular stores, the rapsyn-GCaMP6f fish was crossed with the *relaxed* mutant that lacks functional dihydropyridine receptors (15, 16). Paralytic *relaxed* homozygous fish were used for GCaMP6f monitoring.

Fluorescence response during 0.2-Hz stimulation of the CaP was monitored using a CSU10 spinning confocal microscope (Yokogawa Electric) configured with an ImagEM X2 electron-multiplying charge-coupled device camera (Hamamatsu Photonics). Images were acquired at a rate of 30 frames per second using Micro-Manager software (University of California San Francisco). Frame-by-frame analysis of fluorescence responses was performed in ImageJ (NIH). Individual regions of interest (ROIs) were defined based on the basal fluorescence of GCaMP6f that provided the labeling of synapses. $\Delta F/F_0$ was determined for each ROI, where F_0 represents the prestimulus baseline obtained by averaging 1 s of prestimulus images, and ΔF represents the difference between the fluorescence signal and the baseline ($F - F_0$). Positive responses were identified as peaks greater than 10 times the SD of the baseline signal. Pr was determined as the ratio of the number of positive responses to the total number of stimuli.

Electrophysiology of Neuromuscular Transmission. Paired recordings between Mns and target fast skeletal muscle were performed as previously described for CaP and its muscle target (58). CaPs were identified on the basis of stereotypical morphology and biophysical properties. In light of the large diversity among 2°Mns, we focused on the subset extending branches to both ventral and dorsal muscle targets for quantitation. To identify 2°Mns for recording, we relied on sparse labeling with mnx1:Gal4 and UAS:tdTomato plasmid injection into single-cell embryos or dye filling with 40 μM Alexa Fluor 568 hydrazide in the neuronal recording pipette. The recording bath solution contained 134 mM NaCl, 2.9 mM KCl, 1.2 mM $MgCl_2$, 2.1 mM $CaCl_2$, and 10 mM Na-Hepes, pH 7.8, ~290 mOsm. Both neuron- and muscle-recording pipettes contained 115 mM K-gluconate, 15 mM KCl, 2 mM $MgCl_2$, 5 mM K-ethylene glycol-bis(β-aminoethyl ether)-N,N,N′,N′-tetraacetic acid (EGTA), 10 mM K-Hepes, and 4 mM Mg-ATP, pH 7.2, ~290 mOsm. Action potentials in Mns were elicited by 1-ms current injection, while EPCs were recorded from target muscles voltage-clamped at −50 mV. Muscle-recording pipettes had a resistance of 2 to 5 MΩ and the series resistance was kept under 10 MΩ. All recordings were performed with 60% online series resistance compensation. Synaptic currents were sampled at 100 kHz and filtered at 10 kHz using a HEKA EPC 10/2 amplifier with Patchmaster (HEKA Elektronik). Electrophysiology data were analyzed using Patchmaster and Igor Pro (WaveMetrics). All fish were genotyped after recording.

Exploratory Screening of ω-Conotoxins in ChR-YFP Fish. These experiments were performed in the transgenic line expressing ChR-YFP (yellow fluorescent protein) fusion protein primarily in 2°Mns through a motor neuron-specific GAL4 driver ($Gal4^{s1020t}$; UAS:ChR-YFP, kindly provided by Claire Wyart, University Pierre et Marie Curie, Paris, France). Whole-field light-emitting diode (LED) illumination was used to excite the 2°Mn using a 475-nm LED driver (Thorlabs). Whole-cell currents coupled to 5-ms pulses of optical excitation given at 10-s intervals were monitored continuously in ventral fast skeletal muscle voltage-clamped at −50 mV. Bath solution containing ω-conotoxins (Alomone Labs) was applied directly to the preparation at the indicated concentrations which were based on their effective concentrations for the mammalian N-type channels.

Measurement of Dose-Dependent Response for ω-Conotoxins on Expressed Calcium Channels. Heterologous expression and recording of zebrafish P/Q- and N-type calcium channels were performed as described (18). HEK293T cells were transfected by Lipofectamine 2000 (Invitrogen) with complementary DNAs (cDNAs) for the zebrafish calcium channel α-subunit (accession no. KC192783 for the P/Q channel, KC192784 for the N type), rat α2δ1-subunit (Addgene; accession no. AF286488), and zebrafish β4b-subunit (accession no. KC192785), in equal molar ratio. To help identify transfected cells with fluorescence, we used either an EGFP-tagged α-subunit cDNA or included an empty EGFP vector in the transfection. Cells were replated at low density at 24 h after transfection and recorded within 48 h. Cells with green fluorescence were recorded in the whole-cell voltage-clamp mode with an EPC10/2 amplifier. Patch electrodes (resistances of 3 to 5 MΩ) contained 115 mM Cs methanesulfonate, 15 mM CsCl, 5 mM K-BAPTA, 4 mM Mg-ATP,

and 10 mM Cs-Hepes, pH 7.2 with CsOH, ~280 mOsm. The recording bath solution contained 134 mM NaCl, 2.9 mM KCl, 1.2 mM $MgCl_2$, 2.1 mM $CaCl_2$, and 10 mM Na-Hepes, pH 7.8, ~290 mOsm. The P/Q channel expressed at reduced levels compared with the N type, requiring substitution of Ba^{2+} for Ca^{2+} as the charge carrier (bath solution containing 10 mM $BaCl_2$, 0.2 mM $CaCl_2$). We performed control recordings with Ca^{2+} for comparison. No differences in concentration-dependent block were observed between the two charge carriers ($n = 5$). Whole-cell currents in response to voltage steps were sampled at 100 kHz and filtered at 10 kHz with Patchmaster acquisition software and leak-subtracted online with a p/10 protocol.

For the dose-dependent response, four or five different concentrations of toxins were applied by a quartz micromanifold positioned adjacent to the cell (ALA Scientific Instruments). Since these toxin blocks are reversible, we alternated with perfusion of bath solution, allowing for full recovery to preapplication level before testing the next concentration. After given sufficient time to reach a steady-state block, the current–voltage relationship for each toxin concentration was determined. Peak currents measured with application of toxins were compared with those with bath solution application.

Motility Analysis. Movement was elicited by a 20-ms 50-V stimulus with a Grass SD9 simulator. A stimulus-triggered LED light in the field marked the timing of the stimulus. The evoked motility response was recorded at 1,000 frames per second using a Fastcam 512-PCI camera (Photron). The time course of changes in body curvature was tracked and quantitated using Flote zebrafish motion analysis software (59).

Electron Microscopic Analysis of the Zebrafish NMJ. Wild-type zebrafish larvae (96 to 120 hpf) were high-pressure–frozen and freeze-substituted as described (48). Electron micrographs of 250-nm serial sections were recorded at 200 kV on a JEOL JEM-2100 transmission electron microscope with a TVIPS F416 camera (resolution 2,048 × 2,048).

Data Analysis and Statistical Tests. Data were analyzed using Patchmaster and Igor Pro. Statistical analysis was performed with Prism (GraphPad). Comparisons between two samples were done with a two-tailed *t* test with unequal variances. All data are presented as mean ± SD.

Data Availability. All study data are included in the article.

ACKNOWLEDGMENTS. We thank Dr. Claudia Lopez from the Oregon Health and Science University Multiscale Microscope Core for her help with electron microscopy, and James Kelly for fish care. We are grateful for support with sample preparation to Marlene Strobel, Daniela Bunsen, and Claudia Gehrig-Höhn at the Imaging Core Facility of the Biocenter, University of Würzburg. This work was supported by a grant to P.B. from the NIH.

1. J. R. Fetcho, D. S. Faber, Identification of motoneurons and interneurons in the spinal network for escapes initiated by the Mauthner cell in goldfish. *J. Neurosci.* **8**, 4192–4213 (1988).
2. U. K. Müller, J. L. van Leeuwen, Swimming of larval zebrafish: Ontogeny of body waves and implications for locomotory development. *J. Exp. Biol.* **207**, 853–868 (2004).
3. H. Korn, D. S. Faber, The Mauthner cell half a century later: A neurobiological model for decision-making? *Neuron* **47**, 13–28 (2005).
4. D. W. Liu, M. Westerfield, Function of identified motoneurones and co-ordination of primary and secondary motor systems during zebra fish swimming. *J. Physiol.* **403**, 73–89 (1988).
5. J. R. Fetcho, D. M. O'Malley, Visualization of active neural circuitry in the spinal cord of intact zebrafish. *J. Neurophysiol.* **73**, 399–406 (1995).
6. P. Z. Myers, J. S. Eisen, M. Westerfield, Development and axonal outgrowth of identified motoneurons in the zebrafish. *J. Neurosci.* **6**, 2278–2289 (1986).
7. M. Westerfield, J. V. McMurray, J. S. Eisen, Identified motoneurons and their innervation of axial muscles in the zebrafish. *J. Neurosci.* **6**, 2267–2277 (1986).
8. D. L. McLean, J. Fan, S. Higashijima, M. E. Hale, J. R. Fetcho, A topographic map of recruitment in spinal cord. *Nature* **446**, 71–75 (2007).
9. J. P. Gabriel *et al*., Principles governing recruitment of motoneurons during swimming in zebrafish. *Nat. Neurosci.* **14**, 93–99 (2011).
10. E. Menelaou, D. L. McLean, A gradient in endogenous rhythmicity and oscillatory drive matches recruitment order in an axial motor pool. *J. Neurosci.* **32**, 10925–10939 (2012).
11. S. Bello-Rojas, A. E. Istrate, S. Kishore, D. L. McLean, Central and peripheral innervation patterns of defined axial motor units in larval zebrafish. *J. Comp. Neurol.* **527**, 2557–2572 (2019).
12. W. C. Wang, P. Brehm, A gradient in synaptic strength and plasticity among motoneurons provides a peripheral mechanism for locomotor control. *Curr. Biol.* **27**, 415–422 (2017).
13. P. Brehm, H. Wen, Zebrafish neuromuscular junction: The power of N. *Neurosci. Lett.* **713**, 134503 (2019).
14. H. Wen, M. J. McGinley, G. Mandel, P. Brehm, Nonequivalent release sites govern synaptic depression. *Proc. Natl. Acad. Sci. U.S.A.* **113**, E378–E386 (2016).
15. F. Ono, S. Higashijima, A. Shcherbatko, J. R. Fetcho, P. Brehm, Paralytic zebrafish lacking acetylcholine receptors fail to localize rapsyn clusters to the synapse. *J. Neurosci.* **21**, 5439–5448 (2001).
16. J. Schredelseker *et al*., The beta 1a subunit is essential for the assembly of dihydropyridine-receptor arrays in skeletal muscle. *Proc. Natl. Acad. Sci. U.S.A.* **102**, 17219–17224 (2005).
17. H. Wen *et al*., Distinct roles for two synaptotagmin isoforms in synchronous and asynchronous transmitter release at zebrafish neuromuscular junction. *Proc. Natl. Acad. Sci. U.S.A.* **107**, 13906–13911 (2010).
18. H. Wen *et al*., Zebrafish calls for reinterpretation for the roles of P/Q calcium channels in neuromuscular transmission. *J. Neurosci.* **33**, 7384–7392 (2013).
19. C. Wyart *et al*., Optogenetic dissection of a behavioural module in the vertebrate spinal cord. *Nature* **461**, 407–410 (2009).
20. T. Sakaba, E. Neher, Quantitative relationship between transmitter release and calcium current at the calyx of held synapse. *J. Neurosci.* **21**, 462–476 (2001).
21. M. Dittrich, A. E. Homan, S. D. Meriney, Presynaptic mechanisms controlling calcium-triggered transmitter release at the neuromuscular junction. *Curr. Opin. Physiol.* **4**, 15–24 (2018).
22. A. Brandt, D. Khimich, T. Moser, Few CaV1.3 channels regulate the exocytosis of a synaptic vesicle at the hair cell ribbon synapse. *J. Neurosci.* **25**, 11577–11585 (2005).
23. I. Bucurenciu, J. Bischofberger, P. Jonas, A small number of open Ca^{2+} channels trigger transmitter release at a central GABAergic synapse. *Nat. Neurosci.* **13**, 19–21 (2010).
24. E. Eggermann, I. Bucurenciu, S. P. Goswami, P. Jonas, Nanodomain coupling between Ca^{2+} channels and sensors of exocytosis at fast mammalian synapses. *Nat. Rev. Neurosci.* **13**, 7–21 (2011).
25. K. Sano, K. Enomoto, T. Maeno, Effects of synthetic omega-conotoxin, a new type Ca^{2+} antagonist, on frog and mouse neuromuscular transmission. *Eur. J. Pharmacol.* **141**, 235–241 (1987).
26. E. Katz *et al*., Effects of Ca^{2+} channel blockers on transmitter release and presynaptic currents at the frog neuromuscular junction. *J. Physiol.* **486**, 695–706 (1995).
27. C. Thaler, W. Li, P. Brehm, Calcium channel isoforms underlying synaptic transmission at embryonic *Xenopus* neuromuscular junctions. *J. Neurosci.* **21**, 412–422 (2001).
28. O. D. Uchitel *et al*., P-type voltage-dependent calcium channel mediates presynaptic calcium influx and transmitter release in mammalian synapses. *Proc. Natl. Acad. Sci. U.S.A.* **89**, 3330–3333 (1992).
29. D. Naranjo, H. Wen, P. Brehm, Zebrafish CaV2.1 calcium channels are tailored for fast synchronous neuromuscular transmission. *Biophys. J.* **108**, 578–584 (2015).
30. L. Li, J. Bischofberger, P. Jonas, Differential gating and recruitment of P/Q-, N-, and R-type Ca^{2+} channels in hippocampal mossy fiber boutons. *J. Neurosci.* **27**, 13420–13429 (2007).
31. H. J. Koester, D. Johnston, Target cell-dependent normalization of transmitter release at neocortical synapses. *Science* **308**, 863–866 (2005).
32. T. Éltes, T. Kirizs, Z. Nusser, N. Holderith, Target cell type-dependent differences in Ca^{2+} channel function underlie distinct release probabilities at hippocampal glutamatergic terminals. *J. Neurosci.* **37**, 1910–1924 (2017).
33. N. Holderith *et al*., Release probability of hippocampal glutamatergic terminals scales with the size of the active zone. *Nat. Neurosci.* **15**, 988–997 (2012).
34. Y. Nakamura *et al*., Nanoscale distribution of presynaptic Ca(2+) channels and its impact on vesicular release during development. *Neuron* **85**, 145–158 (2015).
35. E. F. Stanley, The nanophysiology of fast transmitter release. *Trends Neurosci.* **39**, 183–197 (2016).
36. N. Rebola *et al*., Distinct nanoscale calcium channel and synaptic vesicle topographies contribute to the diversity of synaptic function. *Neuron* **104**, 693–710.e9 (2019).
37. H. Sakamoto *et al*., Synaptic weight set by Munc13-1 supramolecular assemblies. *Nat. Neurosci.* **21**, 41–49 (2018).
38. S. Iwasaki, T. Takahashi, Developmental changes in calcium channel types mediating synaptic transmission in rat auditory brainstem. *J. Physiol.* **509**, 419–423 (1998).
39. L. G. Wu, R. E. Westenbroek, J. G. Borst, W. A. Catterall, B. Sakmann, Calcium channel types with distinct presynaptic localization couple differentially to transmitter release in single calyx-type synapses. *J. Neurosci.* **19**, 726–736 (1999).
40. L. Forti, C. Pouzat, I. Llano, Action potential-evoked Ca^{2+} signals and calcium channels in axons of developing rat cerebellar interneurones. *J. Physiol.* **527**, 33–48 (2000).
41. G. J. Stephens, N. P. Morris, R. E. Fyffe, B. Robertson, The Cav2.1/alpha1A (P/Q-type) voltage-dependent calcium channel mediates inhibitory neurotransmission onto mouse cerebellar Purkinje cells. *Eur. J. Neurosci.* **13**, 1902–1912 (2001).
42. S. Hefft, P. Jonas, Asynchronous GABA release generates long-lasting inhibition at a hippocampal interneuron-principal neuron synapse. *Nat. Neurosci.* **8**, 1319–1328 (2005).
43. Y. Q. Cao, R. W. Tsien, Different relationship of N- and P/Q-type Ca^{2+} channels to channel-interacting slots in controlling neurotransmission at cultured hippocampal synapses. *J. Neurosci.* **30**, 4536–4546 (2010).
44. D. Davydova *et al*., Bassoon specifically controls presynaptic P/Q-type Ca(2+) channels via RIM-binding protein. *Neuron* **82**, 181–194 (2014).
45. S. Mochida *et al*., Requirement for the synaptic protein interaction site for reconstitution of synaptic transmission by P/Q-type calcium channels. *Proc. Natl. Acad. Sci. U.S.A.* **100**, 2819–2824 (2003).
46. Z. L. Newman *et al*., Input-specific plasticity and homeostasis at the *Drosophila* larval neuromuscular junction. *Neuron* **93**, 1388–1404.e10 (2017).

47. Y. Akbergenova, K. L. Cunningham, Y. V. Zhang, S. Weiss, J. T. Littleton, Characterization of developmental and molecular factors underlying release heterogeneity at *Drosophila* synapses. *eLife* **7**, e38268 (2018).
48. F. Helmprobst, M. Frank, C. Stigloher, Presynaptic architecture of the larval zebrafish neuromuscular junction. *J. Comp. Neurol.* **523**, 1984–1997 (2015).
49. M. C. Brown, J. K. Jansen, D. Van Essen, Polyneuronal innervation of skeletal muscle in new-born rats and its elimination during maturation. *J. Physiol.* **261**, 387–422 (1976).
50. A. D. Grinnell, Dynamics of nerve-muscle interaction in developing and mature neuromuscular junctions. *Physiol. Rev.* **75**, 789–834 (1995).
51. C. L. Jordan, P. A. Pawson, A. P. Arnold, A. D. Grinnell, Hormonal regulation of motor unit size and synaptic strength during synapse elimination in the rat levator ani muscle. *J. Neurosci.* **12**, 4447–4459 (1992).
52. M. J. Barber, J. W. Lichtman, Activity-driven synapse elimination leads paradoxically to domination by inactive neurons. *J. Neurosci.* **19**, 9975–9985 (1999).
53. S. G. Turney, J. W. Lichtman, Reversing the outcome of synapse elimination at developing neuromuscular junctions in vivo: Evidence for synaptic competition and its mechanism. *PLoS Biol.* **10**, e1001352 (2012).
54. A. C. Dolphin, A. Lee, Presynaptic calcium channels: Specialized control of synaptic neurotransmitter release. *Nat. Rev. Neurosci.* **21**, 213–229 (2020).
55. R. N. Kettleborough *et al*., A systematic genome-wide analysis of zebrafish protein-coding gene function. *Nature* **496**, 494–497 (2013).
56. A. Muto *et al*., Genetic visualization with an improved GCaMP calcium indicator reveals spatiotemporal activation of the spinal motor neurons in zebrafish. *Proc. Natl. Acad. Sci. U.S.A.* **108**, 5425–5430 (2011).
57. T. W. Chen *et al*., Ultrasensitive fluorescent proteins for imaging neuronal activity. *Nature* **499**, 295–300 (2013).
58. H. Wen, P. Brehm, Paired patch clamp recordings from motor-neuron and target skeletal muscle in zebrafish. *J. Vis. Exp.* ((45), 2351 (2010).
59. H. A. Burgess, M. Granato, Modulation of locomotor activity in larval zebrafish during light adaptation. *J. Exp. Biol.* **210**, 2526–2539 (2007).